Soft Matter

PAPER

View Article Online
View Journal | View Issue

Cite this: *Soft Matter*, 2021, **17**, 6160

Cascaded pattern formation in hydrogel medium using the polymerisation approach†

Keita Abe, [a] Satoshi Murata[a] and Ibuki Kawamata *[ab]

Reaction-diffusion systems are one of the models of the formation process with various patterns found in nature. Inspired by natural pattern formation, several methods for designing artificial chemical reaction-diffusion systems have been proposed. DNA is a suitable building block to build such artificial systems owing to its programmability. Previously, we reported a line pattern formed due to the reaction and diffusion of synthetic DNA; however, the width of the line was too wide to be used for further applications such as parallel and multi-stage pattern formations. Here, we propose a novel method to programme a reaction-diffusion system in a hydrogel medium to realise a sharp line capable of forming superimposed and cascaded patterns. The mechanism of this system utilises a two-segment polymerisation of DNA caused by hybridisation. To superimpose the system, we designed orthogonal DNA sequences that formed two lines in different locations on the hydrogel. Additionally, we designed a reaction to release DNA and form a cascade pattern, in which the third line appears between the two lines. To explain the mechanism of our system, we modelled the system as partial differential equations, whose simulation results agreed well with the experimental data. Our method to fabricate cascaded patterns may inspire combinations of DNA-based technologies and expand the applications of artificial reaction-diffusion systems.

Received 26th February 2021,
Accepted 21st April 2021

DOI: 10.1039/d1sm00296a

rsc.li/soft-matter-journal

Introduction

Various types of spontaneous patterns, such as stripes, spots, and wave patterns, are widely observed in nature. For example, animal fur and fish skin patterns are formed due to inter- and intra-cellular communication *via* reaction and diffusion encoded in the gene expression system. Such pattern formation processes can be well represented by a mathematical model expressed as partial differential equations.[1–3] Inspired by those natural patterns, artificial chemical systems built on the reaction-diffusion model can produce certain types of ordered patterns.[4,5]

To expand various pattern formation, it is necessary to programme the reaction and diffusion by tuning various parameters of the chemical reaction systems, such as rate constants and diffusion constants. Synthetic DNA is a useful material for this purpose because of its programmability since interactions among DNA strands can be designed as hybridisation between complementary sequences of nucleotides.[6] The strength of the interactions among DNA sequences can be thermodynamically predicted using efficient algorithms,[7–11] and DNA sequences with desired thermodynamic properties can be computationally designed based on the prediction.[12] Such designed DNA sequences can be chemically synthesised by an automated DNA synthesiser, making DNA a practical building block for artificial reaction systems.[13,14] Various logic circuits proposed in DNA computing demonstrate complex information processing abilities implemented as chemical reactions.[15–20] However, these systems are usually implemented in a well-mixed test tube, and thus, they are limited in utilising spatial inhomogeneity.

Recently, some research on DNA-based artificial reaction-diffusion systems has been reported where spatio-temporal pattern formations have been investigated theoretically and experimentally.[21–32] As a theory, the potential of the DNA-based system was shown in computer simulation research, although it was not realistic to implement as it is.[22–24] In practice, various experimental techniques to realise DNA reaction systems, such as strand displacement, photoresponsive moieties, and various DNA processing enzymes are utilized.[25–29] For instance, propagating waves by amplification reactions, spiral patterns by oscillating reactions,[29] and French flag patterns by activation and inhibition[30] have been demonstrated. Because these reaction-diffusion systems are built-in solutions where the diffusion of molecules is considerably fast, the formed patterns are strongly subject to dissipation. To maintain the formed pattern over time, it is necessary to employ out-of-equilibrium reaction systems that are equally fast as diffusion.

In contrast, various synthetic DNA-based reaction-diffusion systems have been built in a hydrogel material. In hydrogels, the diffusion can be slowed down to the range in which we can

[a] *Department of Robotics, Graduate School of Engineering, Tohoku University, Japan. E-mail: keita.abe.t7@dc.tohoku.ac.jp, satoshi.murata.a4@tohoku.ac.jp, ibuki.kawamata@tohoku.ac.jp*
[b] *Natural Science Division, Faculty of Core Research, Ochanomizu University, Japan*
† Electronic supplementary information (ESI) available. See DOI: 10.1039/d1sm00296a

utilise programmable reactions implemented with DNA. The properties of the DNA reaction can be adjusted by the toehold lengths and base sequences, which is useful to realise desired reaction dynamics for pattern formation. Example patterns formed in the hydrogel medium by DNA include fixed lines, metaboric lines, rings, and detected edges.[25–28,41] Moreover, because the polymer network of the hydrogel medium can completely suppress the diffusion of larger molecules, the formed pattern can be maintained over time after the reaction reaches equilibrium.[25] Another advantage of the hydrogel is that it can be moulded into any shape, and specific DNA species can be immobilised at designated positions in the gel.[25–27,32]

DNA reaction in a hydrogel medium also enables us to programme not only the reaction but also diffusion. We have proposed methods to modulate the diffusion of DNA by using reversible interactions between diffusible DNA and anchored DNA to the gel polymer.[32,33] Combinations between the above methods and enzymatic reactions or DNA logic gates have been realized to construct various long-lived or immobilized patterns.[25,31]

The current research target has been shifted to realize hierarchical pattern formation, that is, the generated patterns in the previous reaction initiate the proceeding reactions for further pattern formation. Although such cascaded pattern formation has been theoretically proposed,[22–24] experimental implementation remains quite challenging owing to the smaller reaction rate and lower yield,[34,35] which results in a blurred pattern, making it difficult to distinguish several patterns in the near distance.

Here, we propose a novel method to design a DNA reaction–diffusion system for a cascaded pattern formation. Utilising a two-segment polymerisation of DNA, in which two types of single-stranded DNA alternately hybridise with each other to assemble a long double-stranded DNA, the molecule can be trapped in a narrow area in the hydrogel. This method enabled the formation of distinguishable sharper patterns compared with conventional methods. Using orthogonal DNA sequences, we created two independent patterns superimposed on the same hydrogel, which were then used to generate the next pattern using the same two-segment polymerisation strategy. The strategy was successfully demonstrated in a one-dimensional experiment, the results of which were well-modelled using partial differential equations and explained by numerical simulations.

Our method of cascaded pattern formation can be combined with other techniques for controlling chemical and physical properties of a material through DNA interactions (*i.e.* beads-beads interactions,[53] crosslink density,[48] or production of enzymes[54]). If we can further materialise the formed pattern (*i.e.* beads aggregations and gel–sol transition), it may facilitate the realisation of an artificial system that spontaneously builds its structure, similar to biological development.

Material and methods

DNA solutions

Unmodified DNA with OPC (Oligonucleotide Purification Cartridge) purification was purchased from Eurofins Genomics Japan. Fluorescent-labelled DNA with HPLC purification was purchased from Sangon Biotech Co., Ltd China, except for the FAM-labelled DNA for fluorescence recovery after photobleaching (FRAP) experiment. The exceptional DNA with OPC purification quality was also purchased from Eurofins Genomics. These DNA sequences are detailed in Fig. S1 and Table S1 (ESI†). All the DNAs were diluted in Milli-Q water to a concentration of 100 μM and stored at −30 °C.

The reaction buffer contained 50 mM HEPES, 20 mM $MgCl_2$, and 100 mM NaCl (pH 7.13). To prepare the hydrogel medium, a pre-gel solution was prepared by mixing the reaction buffer, 40% acrylamide, and 2% *N*,*N*′-methylenebis (acrylamide) to make a 10% polyacrylamide gel (*C*% = 5) containing the buffer. For gelation, immediately after mixing 0.1% APS and 0.1% TEMED, we applied the solution into a mould (Fig. S2, ESI†) while preventing bubbles, setting a comb, and incubating it at room temperature (25 °C) for 1 h. All reagents were purchased from FUJIFILM Wako Pure Chemical Corporation, Osaka, Japan, except 40% acrylamide, 2% *N*,*N*′-methylenebis (acrylamide) (Bio-Rad Laboratories, Inc.), and NaCl (Sigma Life Science). The final concentration and the volume of DNA applied in the pocket of the hydrogel were 10 μM and 4 μL, respectively.

Imaging with fluorescent microscopy

We visualised the reaction field using a Nikon TE2000 U with four types of filter units for four channels of fluorescent observation (FAM, Cy5, AMCA, and Cy3). Imaging of one reaction field was performed at intervals of 10 min over 24 h. In practice, by facilitating an automated stage (Shiguma Koki, Japan), five reaction fields were imaged in parallel.

Image composition

Pseudo-colour images were obtained from the grey scale images of the reaction field. Bisector pattern formation was visualised from the FAM and Cy5 images, assigning them to green and magenta channels, respectively. Stripe pattern formation was visualised by merging the FAM (green) and AMCA (blue) images (Fig. S3, ESI†). In the cascaded pattern formation, Cy5 was used for both R1 and R3 DNAs, whereas Cy3 was used for both R2 and L3 DNAs. Thus, the distribution of pair 3 was visualised from Cy5 and Cy3 images using the ''Multiply'' function of ImageJ.[36] The resultant image was assigned to a red channel composed of a visualised image with other channels of FAM (green) and AMCA (blue) (Fig. S4, ESI†).

FRAP experiment

We performed the FRAP experiment to measure the diffusion coefficients of DNA in a 10% polyacrylamide gel. The gel prepared in a tube with a volume of 10 μL was placed on a silicon chamber, covered with liquid paraffin to prevent evaporation, and photo-stimulated using a TE-3000 confocal unit attached to Olympus IX83 (Fig. S5, S6 and Table S2, ESI†).

Reaction-diffusion simulation

For the reaction-diffusion simulation, we employed the executable file ''rdy.exe'' packaged in a reaction-diffusion simulator Ready.[37]

The simulations were performed in an Elite Desk800 G4 SFF (Hewlett-Packard) equipped with NVIDIA FGeForce GTX 1650 for bisector pattern formation, or DAIV-DGX760H2-M2S5 (Mouse Computer) equipped with NVIDIA GeForce RTX 2080 for stripe and cascaded pattern formations. From Visual Toolkit Image Data (vti) formatted results of simulations, numerical information such as concentration distribution was obtained using the visual toolkit (vtk) library[38] of Python.

Result and discussion

DNA polymerisation for bisector pattern formation

We programmed a reaction–diffusion system wherein two types of DNAs diffuse and hybridise with each other somewhere around the centre (Fig. 1). In the programme, we employed a polymerisation approach, which is a method to immobilise DNA in a hydrogel medium as a result of polymer formation by hybridisation. We implemented the programme using polyacrylamide gel and fluorescent-labelled DNA. The moulded gel with two pockets 3 mm apart, was placed on a microscope stage (Fig. 1a). We applied a 4 μL solution containing DNA into the pockets and used them as initial sources.

A 46 nt of single-stranded DNA named L1 was placed in the left pocket, whereas another 46 nt single-stranded DNA named R1 was placed in the right pocket. For observation, L1 and R1 were modified with FAM (green) and Cy5 (magenta), respectively. They diffuse in the hydrogel medium (Fig. S8, ESI†), and when they encounter, they hybridise through 23 nt domains complementary to each other (Fig. 1b). This hybridisation repeats alternately as long as both DNA strands are present, forming a double-stranded DNA polymer (Fig. 1c). The polymer becomes longer as the hybridisation continues, and its diffusion coefficients become smaller following the Stokes–Einstein equation.[39]

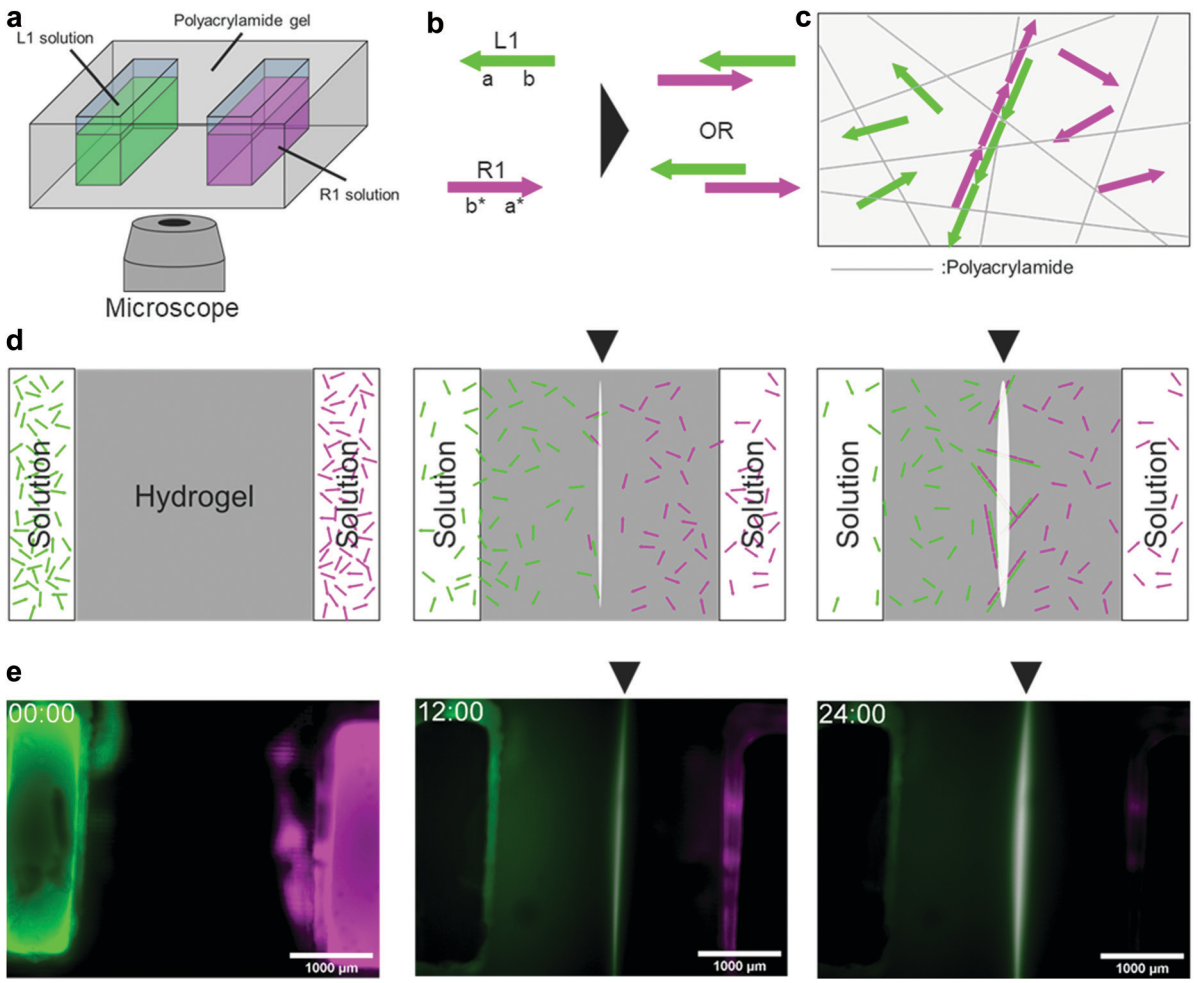

Fig. 1 Polymerization approach for pattern formation. (a) Schematics of experimental setup. A polyacrylamide hydrogel with DNA solutions in two pockets is placed on a microscopy stage. (b) Two types of hybridization between L1 and R1. Domain level representation of L1 and R1 are ''ba'' and ''a*b*'', respectively, where * means the complementary domains. (c) Polymerization of L1 and R1 in hydrogel. The polymer is immobilized in the hydrogel when its size is large. (d) Step-by-step (left to right) pattern formation process between two pockets. The triangle mark represents the position of the line. (e) Snapshots from fluorescent microscopy observation of the pattern formation after 0, 12, and 24 h from the beginning of the observation. Scale bar is 1000 μm.

Consequently, the DNA polymer was immobilised on a polyacrylamide hydrogel (Fig. 1c and d).

In 24 h of fluorescent observation, a white line appears on the bisector between the source pockets(Fig. 1e). As white is the composition of green (FAM) and magenta (Cy5), the white area represents the colocalisation of L1 (FAM-labelled) and R1 (Cy5-labelled). The white line appeared at the midpoint between the pockets because L1 and R1 had the same number of bases and diffused at approximately the same speed. This result suggests that the programme for bisector pattern formation works successfully.

Superimposed pattern formation using adjuster DNA and orthogonal DNA pairs.

It is possible to shift the position of the white line by changing the diffusion speeds of L1 and R1. For example, when L1 diffuses slower than R1, polymerisation occurs closer to the L1 source. Therefore, a line appears on the left side of the bisector.

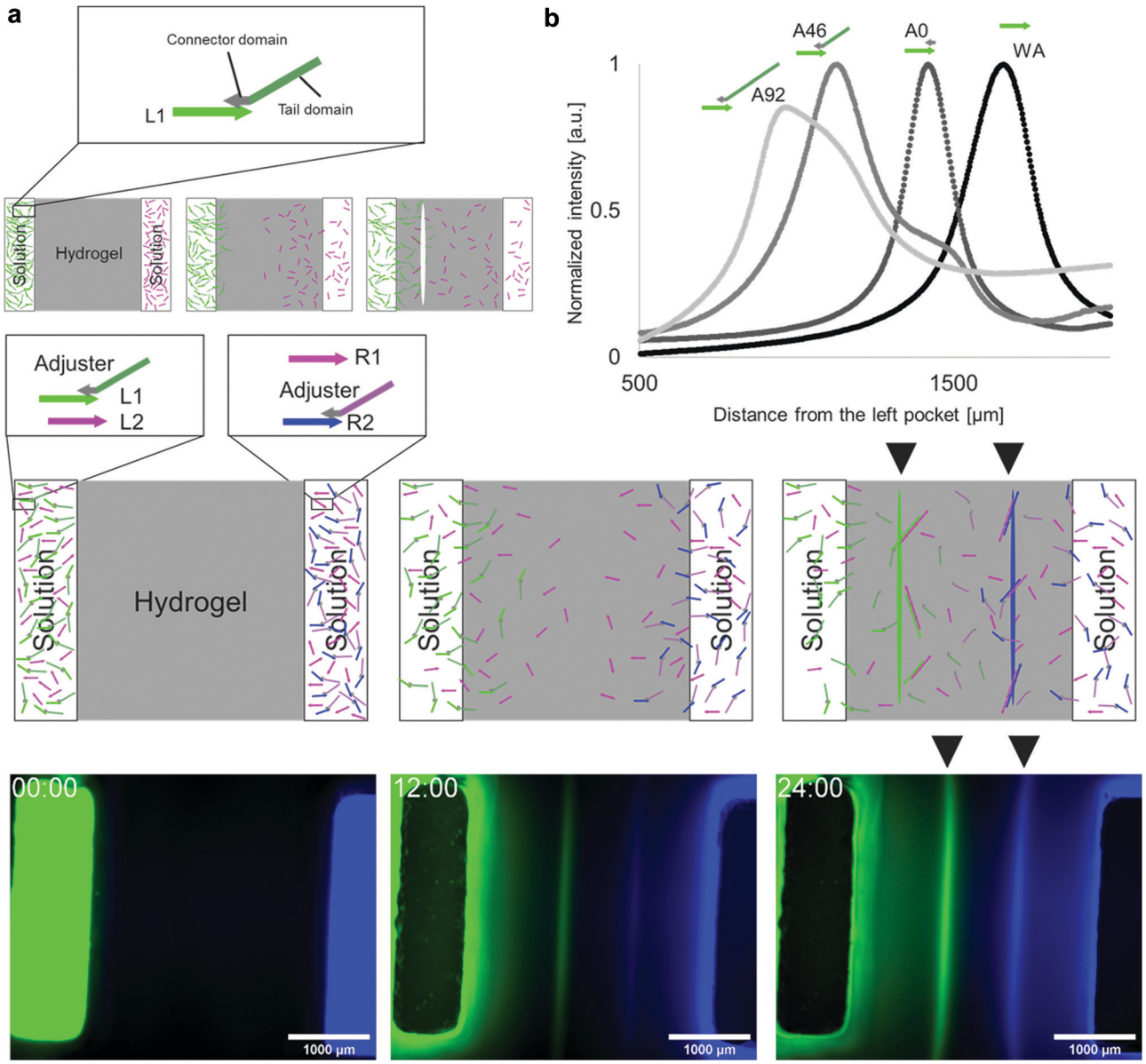

Fig. 2 Adjuster DNA and superimposed pattern. (a) Adjuster DNA has a connector domain for hybridization with L1 and a tail domain for modulating diffusion by tuning its length. As a result of the diffusion modulation, the position of the formed line is shifted to the left. (b) Relationship between the tail length and the position of the lines. The horizontal axis is the distance from the left pocket. The vertical axis is the normalized geometric means of fluorescent intensity of FAM (labeled to L1) and Cy5 (labeled to R1). (c) Schematics of superimposed pattern formation. L2 and R2 have orthogonal base sequences with L1 and R1, which hybridize, make polymers, and form another pattern similar to L1 and R1. Initially, L1 with an adjuster and L2 are in the left pocket, and R1 and R2 with an adjuster are in the right pocket. Consequently, two lines appear because L1 and R1 form polymer at the left side (Green), whereas L2 and R2 form at the right side (Blue). (d) Snapshots from fluorescent microscopy observation of the superimposed pattern formation after 0, 12, and 24 h. The scale bar is 1000 μm.

To tune the DNA diffusion speed, we introduced adjuster DNAs. The adjuster hybridises with L1 DNA *via* a connector domain and slows down the diffusion because it increases the net molecular size. The adjuster also has a tail domain for tuning the molecular size (Fig. 2a). As the connector domain (15 nt) is shorter than the base pairs created by the hybridisation between L1 and R1 (23 bp), the adjuster can be released by a strand displacement reaction[15,35] when the polymerisation process takes place.

We prepared three types of adjusters with 0, 46, and 92 nt tail lengths (A0, A46, and A92, respectively) and measured the line positions (Fig. 2b). The line positions from the left source, without the adjuster, A0, A46, and A92 were $(1.65 \pm 0.03) \times 10^3$ μm, $(1.27 \pm 0.07) \times 10^3$ μm, $(1.05 \pm 0.05) \times 10^3$ μm, and $(0.98 \pm 0.02) \times 10^3$ μm, respectively. Longer tails cause the line position to shift to the left as expected, which indicates the effectiveness of the diffusion tuning.

To demonstrate the multiple pattern formation superimposed in the same field, an additional DNA pair (pair 2 (L2 and R2)), which is orthogonal[40] to pair 1 (L1 and R1), was designed (Fig. 2c). L1 and L2 were placed in the left source, whereas R1 and R2 were in the right source. Using the adjuster, the diffusion of L1 and R2 was set to be slower than that of R1 and L2.

L2 and R2 were modified with Cy3 and AMCA, respectively, and the distributions of the two DNA pairs were visualised by four-channel fluorescent observation. When the fluorescence images of FAM and AMCA were assigned to the green and blue channels in Fig. 2d, two lines appeared within 24 h. The results clearly show that the patterns formed by pairs 1 and 2 are formed in the left and right positions, respectively, as expected, indicating that orthogonal pairs can react independently.

Cascaded pattern formation

The DNA reaction–diffusion system can be cascaded in such a way that a formed pattern is used as a source of DNA in subsequent pattern formation. We designed a system that uses the previous two lines for third-line pattern formation. In the system, L1 and R2 are hybridised with adjusters L3 and R3, respectively, through 15 nt connector domains. The 46 nt tail domains of L3 and R3 have new base sequences for the third two-segment polymerization, which are orthogonal to the sequence of pairs 1 and 2 DNAs. During the polymerization of left (pair 1) and right (pair 2) lines, L3 and R3 are released and then form the centre line (pair 3) between the two (Fig. 3a).

In the fluorescent observation, L1, R1, L2, R2, L3, and R3 were modified with FAM, Cy5, Cy3, AMCA, Cy3, and Cy5, respectively, and the results were composed by assigning FAM, AMCA, and (merged Cy3 and Cy5) to green, blue, and red, respectively. After 12 h, yellow (green + red) and magenta (blue + red) lines appeared, after which a red line appeared between them (Fig. 3b). The intensity of left and right lines reached 0.05 at 22.5 h and 18.5 h, respectively, then the centre line appeared at 23.5 h (Fig. 3c). In the case of a non-cascaded process using the same pair 3 as in the centre line (Fig. S7, ESI†), the intensity is reached the same level at 15 h. This experimental result indicates successful pattern formation using a cascaded reaction-diffusion system.

Simulation of non-cascaded, superimposed, and cascaded pattern formation

These three types of pattern formations were compared with the results of the reaction–diffusion simulation. In the simulation, the polymerisation process was modelled as a set of chemical

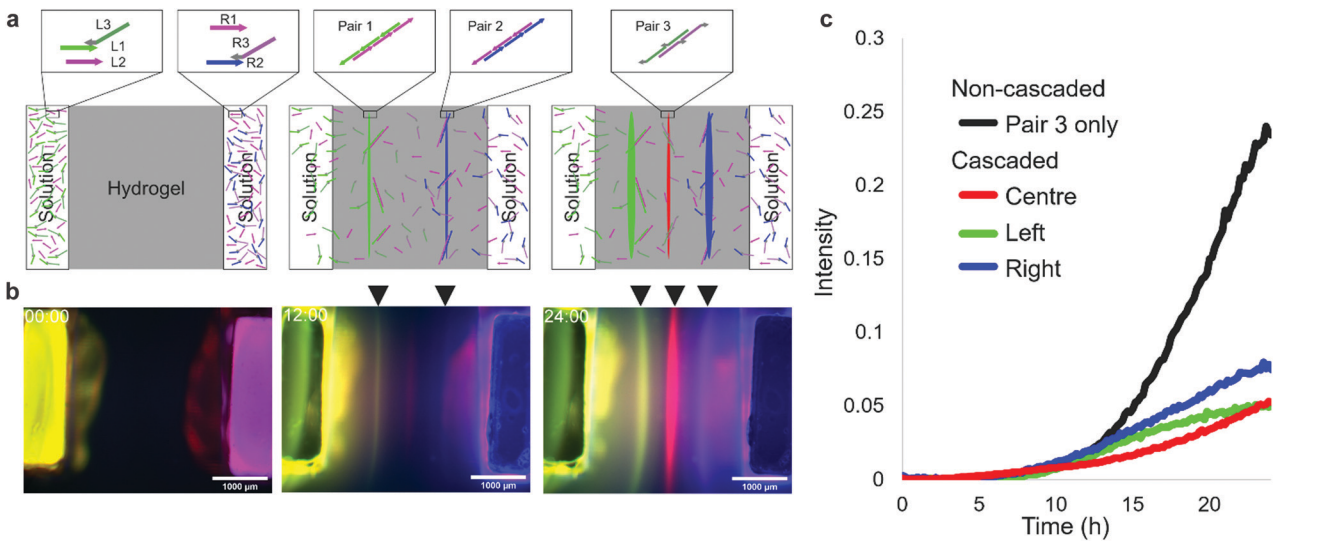

Fig. 3 Cascaded pattern formation. (a) Schematics of cascaded pattern formation. L3 and R3 act as adjusters for L1 and R2, respectively. Initially, L1 with L3 and L2 are in the left pocket and R1 and R2 with R3 are in the right pocket. By the same mechanism of superimposed pattern formation, green and blue lines are formed by which L3 and R3 are released, respectively. Therefore, an additional red line appears between the two lines by the polymerization of L3 and R3. (b) Snapshots from fluorescent microscopy observation of the cascaded pattern formation after 0, 12, and 24 h. The scale bar is 1000 μm. (c) Growth of the centerline. The *x*-axis represents time. The *y*-axis represents the normalized fluorescence intensity at the position that gives the peak of fluorescent distribution in each timestep. The intensity is normalized to the raw fluorescence intensity in the pocket at 0 h as 1.

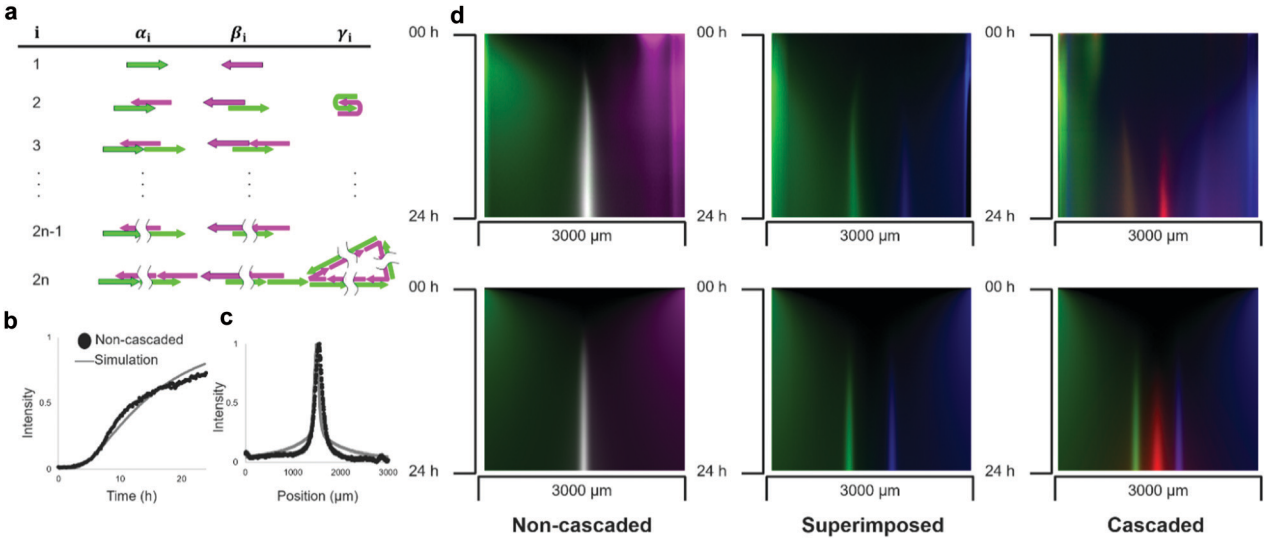

Fig. 4 Reaction-diffusion simulation for the pattern formations. (a) Classification of DNA polymers into α, β, and γ with respect to the number of DNA strands in polymers. Here, the left-most single stranded part of group α and β are labeled L1 and R1(bordered strands), respectively. Circular polymers are classified as γ. (b) Growth of the line in experiment and simulation. The x-axis represents time. The y-axis represents the normalized fluorescence intensity at the position that gives the peak of the fluorescent distribution at 24 h. The intensity is normalized to the raw fluorescence intensity in the pocket at 0 h as 1. (c) Shape of pattern between the pockets after 24 h. The horizontal axis is the distance from the left pocket. The vertical axis is the normalized fluorescence intensity. (d) Kymographs of non-cascaded, superimposed, and cascaded pattern formation of experiment and simulation. The horizontal axis is the distance from the left pocket and the vertical axis is the time from the start of observation.

reactions in which molecular species are intermediate polymerisation products. The products were classified into three groups according to their reactivity characterised by a left-most sticky end (Fig. 4a): the group α has 5′ end of L1, the group β has 3′ end of R1, and group γ is a circular polymer.

The number of DNA strands in a polymer determines the size of the molecule. As the polymerisation process continues unlimitedly, we set N as the maximum number of strands to limit the structure enumeration. Based on the comparison with the electrophoresis results (Fig. S1, ESI†), $N = 16$ was used in the simulation. In the model, hybridisation of complementary single-stranded domains among intermediate structures was considered as a reaction (S5). The diffusion was modelled as a concentration-based isotropic spreading of molecules, where the diffusion coefficient of the intermediate structure was inversely related to the number of strands, which agrees with the Stokes–Einstein theory.[39] The partial differential equations of the model were solved numerically.

Parameters such as rate constants and diffusion coefficients were determined by fitting the simulation curves to the experimental data (Fig. S7, ESI†). We assumed that the experimentally observed fluorescence intensity is proportional to the sum of the concentrations of intermediate structures multiplied by the number of fluorescent-labelled DNA. To fit the simulation, we compared the time development of the non-cascaded pattern between the experiment and simulation (Fig. 4b). For simplicity, a comparison was made only for the position that gives the concentration peak at 24 h. The obtained hybridisation constant was $k_h = 3.5 \times 10^{-4}$ M^{-1} s^{-1}, the diffusion coefficient of single-stranded DNA was $D_1 = 20$ μm^2 s^{-1}, and the rate constant of intramolecular hybridisation was $k_c = 3.0 \times 10^{-3}$ s^{-1}. We think the value of diffusion coefficient is reasonable because it has the same order of magnitude with the values obtained by FRAP analysis (Table S2, ESI†). For example, the relative error between the experiment and simulation results that gives 0.5 fluorescent intensities was less than 9%.

To compare the pattern formed after 24 h in the experiment and simulation, the geometric means of the fluorescent intensities of L1 and R1 were plotted (Fig. 4c). As expected, the simulation results agree with the experimentally formed pattern. Quantitatively, the positions of the peaks were 1.55 and 1.50 mm in the experiment and simulation, respectively, giving a relative error of less than 4%. We further quantified the relative error of the half-width of the curve, which was 31% (1.8×10^2 and 1.4×10^2 μm in the experiment and simulation, respectively).

To simulate the superimposed and cascaded pattern formations, we created similar models. In the case of the superimposed pattern, almost the same polymerisation process takes place, except for the reaction of displacing adjuster strands. The rate constant of the hybridisation reaction in the model, which changed to this displacement reaction, is substituted with k_s from k_h. The kymographs of the fluorescence distribution between the pockets show that the simulation successfully agreed with the experiments (Fig. 4d).

Conclusions

We have proposed a simple but novel method that utilises the DNA polymerisation approach to form sharp line patterns in a hydrogel medium. The programmability of the position of the

formed lines was demonstrated by implementing reaction–diffusion systems employing adjuster DNA strands.

Our polymerisation approach, which requires three DNA strands, is concise compared with the conventional methods that form similar line patterns based on DNA reaction–diffusion systems with seven[26] and eleven strands.[25] The half-widths of the lines formed by our method were significantly sharper than those of the other methods. The value was 181 μm (6% of the distance between two sources) compared to 842 μm, which is 55% of the source distance in the conventional method.[25]

These improvements made it possible to design orthogonal DNA sequences to form multiple patterns in parallel and in sequence. As demonstrations, we succeeded in realising superimposed and cascaded pattern formations in which two lines appeared simultaneously, and an additional line appeared between them.

To validate the polymerisation approach results in pattern formation, we modelled and simulated a DNA reaction–diffusion system based on partial differential equations. The agreement between the simulation and experimental results suggests that the pattern formation behaviour is ascribed to the designed reaction and diffusion of DNA.

As the polymerisation approach is driven by DNA hybridisation reactions, this method is compatible with other DNA-based systems such as enzymatic reactions[42,43] and DNA hydrogel.[41,44–48] For example, if sufficient DNA can be supplied, gel–sol transition of DNA material may be possible.[55] As potential applications of this cascaded pattern formation, we can anticipate building artificial systems that autonomously construct their own structures, mimicking the pattern formation process seen in the development of living organisms.[49] In the morphogenesis of flies, stripe patterns are formed step by step from a simple concentration gradient, and body segments are materialised based on this pattern.[50] Inspired by these processes, we assume that the cascaded pattern formation can be combined with other technologies that control the concentration of other functional molecules, such as enzymes, and change the physical properties of the hydrogel medium.[51,52]

Author contributions

K. A., S. M., and I. K. conceived and developed the project. K. A. performed experiments and computer simulations. K. A., S. M., and I. K. analyzed and interpret the data and wrote the manuscript.

Conflicts of interest

There are no conflicts of interest to declare.

Acknowledgements

This work was supported by JSPS KAKENHI Grant Numbers JP18K18144, JP19KK0261, JP20H05971, JP20H00618, JP20K20979, JP20H05969, JP19J20990.

References

1 A. M. Turing, *Philos. Trans. R. Soc. London*, 1952, **B237**, 37–72.
2 S. Kondo and R. Asai, *Nature*, 1995, **376**(6543), 765.
3 S. Kondo and T. Miura, *Science*, 2010, **329**(5999), 1616–1620.
4 A. Adamatzky and B. L. Costello, *Phys. Lett. A*, 2003, **309.5-6**, 397–406.
5 A. Sirimungkala, H. D. Försterling, V. Dlask and R. J. Field, *J. Phys. Chem. A*, 1999, **103**(8), 1038–1043.
6 J. D. Watson and F. H. Crick, *Nature*, 1953, **171.4356**, 737–738.
7 J. Santalucia, H. T. Allawi and P. A. Seneviratne, *Biochemistry*, 1996, **35.11**, 3555–3562.
8 J. Santalucia, *Proc. Natl. Acad. Sci. U. S. A.*, 1998, **95.4**, 1460–1465.
9 N. Sugimoto, S. Nakano, M. Yoneyama and K. Honda, *Nucleic Acids Res.*, 1996, **24**(22), 4501–4505.
10 D. Y. Zhang and E. Winfree, *J. Am. Chem. Soc.*, 2009, **131**(47), 17303–17314.
11 M. Zuker, *Nucleic Acids Res.*, 2003, **31.13**, 3406–3415.
12 J. N. Zadeh, C. D. Steenberg, J. S. Bois, B. R. Wolfe, M. B. Pierce, A. R. Khan and N. A. Pierce, *J. Comput. Chem.*, 2011, **32**(1), 170–173.
13 X. Song and J. Reif, *ACS Nano*, 2019, **13**(6), 6256–6268.
14 C. Zhang, L. Ge, Y. Zhuang, Z. Shen, Z. Zhong, Z. Zhang and X. You, *Sci. China Inf. Sci.*, 2019, **62**(6), 61301.
15 D. Soloveichik, G. Seelig and E. Winfree, *Proc. Natl. Acad. Sci. U. S. A.*, 2010, **107**(12), 5393.
16 A. Okamoto, K. Tanaka and I. Saito, *J. Am. Chem. Soc.*, 2004, **126**(30), 9458–9463.
17 X. Chen, *J. Am. Chem. Soc.*, 2011, **134**(1), 263–271.
18 Q. Lulu and E. Winfree, *Science*, 2011, **332.6034**, 1196–1201.
19 N. Shimada, K. Saito, T. Miyata, H. Sato, S. Kobayashi and A. Maruyama, *Adv. Funct. Mater.*, 2018, **28**(17), 1707406.
20 K. M. Cherry and L. Qian, *Nature*, 2018, **559**(7714), 370–376.
21 K. Abe and S. Murata, *New Gener Comput.*, 2020, **38**, 379–393.
22 D. Scalise and R. Schulman, *Technology*, 2014, **2**(01), 55–66.
23 I. Kawamata, S. Yoshizawa, F. Takabatake, K. Sugawara and S. Murata, *International Conference on Unconventional Computation and Natural Computation*. Springer, Cham, 2016. pp. 168–181.
24 I. Kawamata, T. Hosoya, F. Takabatake, K. Sugawara, S. M. Nomura, T. Isokawa, F. Peper, M. Hagiya and S. Murata, *2016 Fourth International Symposium on Computing and Networking (CANDAR)*. IEEE, 2016. pp. 215–221.
25 K. Abe, I. Kawamata, S. M. Nomura and S. Murata, *Mol. Syst. Des. Eng.*, 2019, **4.3**, 639–643.
26 J. Zenk, D. Scalise, K. Wang, P. Dorsey, J. Fern, A. Cruz and R. Schulman, *RSC Adv.*, 2017, **7**(29), 18032–18040.
27 S. Chen and G. Seelig, *Soft Matter*, 2020, **16**(14), 3555–3563.
28 S. M. Chirieleison, P. B. Allen, Z. B. Simpson, A. D. Ellington and X. Chen, *Nat. Chem.*, 2013, **5**(12), 1000.
29 A. Padirac, T. Fujii, A. Estévez-Torres and Y. Rondelez, *J. Am. Chem. Soc.*, 2013, **135**(39), 14586–14592.
30 A. S. Zadorin, Y. Rondelez, G. Gines, V. Dilhas, G. Urtel, A. Zambrano and A. Estévez-Torres, *Nat. Chem.*, 2017, **9**(10), 990.
31 G. Urtel, A. Estevez-Torres and J. C. Galas, *Soft Matter*, 2019, **15**(45), 9343–9351.

32 T. Hosoya, I. Kawamata, S. M. Nomura and S. Murata, *New Gener. Comput.*, 2019, **37**(1), 97–111.
33 T. Rodjanapanyakul, F. Takabatake, K. Abe, I. Kawamata, S. M. Nomura and S. Murata, *Phys. Rev. E*, 2018, **97**(5), 052617.
34 B. Yurke, A. J. Turberfield, A. P. Mills, F. C. Simmel and J. L. Neumann, *Nature*, 2000, **406**(6796), 605–608.
35 N. Srinivas, J. Parkin, G. Seelig, E. Winfree and D. Soloveichik, *Science*, 2017, **358**(6369), eaal2052.
36 C. T. Rueden, J. Schindelin, M. C. Hiner, B. E. DeZonia, A. E. Walter, E. T. Arena and K. W. Eliceiri, *BMC Bioinf.*, 2017, **18**(1), 1–26.
37 T. Hutton, R. Munafo, A. Trevorrow, T. Rokicki and D. Wills, Ready, a cross-platform implementation of various reaction-diffusion systems, https://github.com/GollyGang/ready.
38 https://vtk.org/.
39 A. Einstein, [AdP 17, 549 (1905)], *Ann. Phys.*, 2005, **14.S1 1**, 182–193.
40 T. Kitajima, M. Takinoue, K. I. Shohda and A. Suyama, *International Workshop on DNA-Based Computers*. Springer, Berlin, Heidelberg, 2007. pp. 119–129.
41 P. J. Dorsey, D. Scalise and R. Schulman, *Angew. Chem.*, 2021, **133.1**, 342–348.
42 K. Montagne, R. Plasson, Y. Sakai, T. Fujii and Y. Rondelez, *Mol. Syst. Biol.*, 2011, **7.1**, 466.
43 T. Fujii and Y. Rondelez, *ACS Nano*, 2013, **7.1**, 27–34.
44 F. Li, D. Lyu, S. Liu and W. Guo, *Adv. Mater.*, 2020, **32**(3), 1806538.
45 D. Kandatsu, K. Cervantes-Salguero, I. Kawamata, S. Hamada, S. M. Nomura, K. Fujimoto and S. Murata, *ChemBioChem*, 2016, **17**(12), 1118–1121.
46 D. C. Lin, B. Yurke and N. A. Langrana, *J. Biomech. Eng.*, 2004, **126.1**, 104–110.
47 Z. Zhu, C. Wu, H. Liu, Y. Zou, X. Zhang, H. Kang and W. Tan, *Angew. Chem., Int. Ed.*, 2010, **49**(6), 1052–1056.
48 A. Cangialosi, C. Yoon, J. Liu, Q. Huang, J. Guo, T. D. Nguyen and R. Schulman, *Science*, 2017, **357**(6356), 1126–1130.
49 L. Wolpert, T. Cheryll and A. M. Arias, *Principles of Development*, Oxford University Press, USA, 2015.
50 D. St Johnston and C. Nüsslein-Volhard, *Cell*, 1992, **68**(2), 201–219.
51 M. Lovrak, W. E. Hendriksen, C. Maity, S. Mytnyk, V. van Steijn, R. Eelkema and J. H. van Esch, *Nat. Commun.*, 2017, **8**, 15317.
52 M. Lovrak, W. E. Hendriksen, M. T. Kreutzer, V. van Steijn, R. Eelkema and J. H. van Esch, *Soft Matter*, 2019, **20**, 20.
53 W. Zhao, W. Chiuman, M. A. Brook and Y. Li, *ChemBioChem*, 2007, **8**(7), 727–731.
54 Y. J. Chen, B. Groves, R. A. Muscat and G. Seelig, *Nat. Nanotechnol.*, 2015, **10**(9), 748–760.
55 G. Zanchetta, *Curr. Opin. Colloid Interface Sci.*, 2019, **40**, 1–13.